

Shaking table test of a multi-story subway station under pulse-like ground motions



Zhiyi Chen^{a,b,*}, Wei Chen^b, Yueyang Li^b, Yong Yuan^{a,b}

^a State Key Laboratory of Disaster Reduction in Civil Engineering, Tongji University, Shanghai 200092, China

^b Department of Geotechnical Engineering, Tongji University, Shanghai 200092, China

ARTICLE INFO

Article history:

Received 13 April 2015

Received in revised form

16 November 2015

Accepted 7 December 2015

Keywords:

Shaking table test

Multi-story subway station

Pulse-like ground motion

Dynamic responses

ABSTRACT

A series of shaking table tests were conducted to investigate the effect of pulse-like ground motion on a multi-story subway station. Dynamic response data, including internal forces, column drift, and settlement and deformation of the soil were obtained and analyzed. Results show that the pulse-like ground motion increases dynamic responses of the subway station and surrounding soils mainly owing to its inherent rich low-frequency component and high energy. In terms of the structure, central columns, especially central columns on a floor with large story height, are vulnerable components of a multi-story subway station. Both the dynamic earth pressure and the deformation mode of the side wall were analyzed.

© 2015 Elsevier Ltd. All rights reserved.

1. Introduction

With the rapid development of the economy and society in China, modern underground transportation, represented by the subway, is continuously developing towards having a deeper and multilevel structural form. Huaihai Road Station on metro line 13 in Shanghai, for example, is a six-story island-platform station having height of nearly 30 m and diaphragm walls that are 71 m deep [1]. More problems tend to arise for a deeper structural form that has multiple layers and a larger story height. First, the water and earth pressures imposed on side walls of the structure increase with an increase in depth. Second, owing to the accumulation of load transferred from top to bottom, the axial compression ratio of central columns increases. Third, the structural configuration tends to be more complicated so as to provide multiple functions, which increases the number of latent vulnerable points. Finally, a large story height greatly reduces the lateral stiffness of central columns and side walls. Hence, the seismic performance of such an underground structure is worthy of attention.

In recent years, centrifuge and shaking table tests have been conducted for subway stations to study the seismic performance and failure mechanism of their underground structures [2–5]. Results show that underground structures may suffer severe

damage during a strong earthquake. It is commonly believed that the centrifuge test is an attractive way for seismic performance evaluations due to its ability of reproducing the in-site stress state of soils. Researches have been conducted by using a centrifuge, and good results were obtained [6,7]. In addition, shaking table is subtlety in loading, control and observation [8]. Hence, shaking table test is also a common way for studying seismic performance of underground structures [6,9,10]. These studies are of great help to understand soil–structure interaction or responses of structures.

In studies of superstructures, it is also found that pulse-like ground motions may induce more severe damage to structures compared with other ground motions, such as far-field ground motions. Pulse-like ground motion is defined as ground motion whose PGV/PGA (the ratio of peak ground velocity to peak ground acceleration) is greater than 0.2 while ordinary ground motion has a ratio smaller than 0.15 [11]. If the rupture propagates in the direction of the recording station, coherently traveling long-period waves produce high ground velocities and large displacements in the fault-normal direction [12], and most of the seismic energy in ground motion is concentrated in the pulse [13]. Many studies have verified the effects of pulse-like ground motion on the superstructure. Bertero et al. [14] showed that pulse-like ground motion can induce a dramatically strong response in fixed-base buildings. Anderson and Bertero [15], in their study of the non-linear dynamic response of a 10-story steel frame, revealed that the lower floors of buildings with such structure can suffer great damage if subjected to pulse-like ground motion. Makris and Black [16] found that local, distinguishable acceleration pulses result in unusual demands of structures. Sehhati et al. [17] stated that

* Corresponding author at: Department of Geotechnical Engineering, Tongji University, Shanghai 200092, China.

E-mail address: zhiyichen@tongji.edu.cn (Z. Chen).

pulse-like ground motions impose a larger ductility demand on a structure compared with ordinary ground motions. Additionally, studies have been conducted on the effect of pulse-like ground motions on isolated structures and bridges [18–22]. With regard to underground structures, Chen and Wei [23] studied the effect of pulse-like ground motion on mountain tunnels and concluded that the velocity pulses are the main factor determining damage to tunnel linings. However, from the perspective of the structural form, the subway station has a framed structure. Hence, the subway station and tunnel differ in terms of their mechanical and vibration characteristics. Furthermore, the framed structure configuration does not transmit static loads as effectively as a circular lining. As a result, the high-energy impulse of pulse-like ground motion poses a great threat to the structural members of a framed structure, doing damage to the undetected vulnerable spots and even to the whole structure. Additionally, the impulse may increase the shear deformation of soil notably and thus enlarge the story drift of the station and cause further damage.

In this paper, shaking table tests of a multi-story subway station under pulse-like ground motions are conducted. On the basis of the elastic response of a subway station under different ground motions, the effects of pulse-like ground motion on the internal force and deformation of structural members are discussed. The dynamic earth pressure and deformation pattern of the side wall are investigated. Moreover, the seismic performance of a deep subway station under different levels of ground motion are evaluated.

2. Experimental setup

2.1. Shaking table

The shaking table test was carried out using the MTS Company shaking table facility at the State Key Laboratory for Disaster Reduction in Civil Engineering, Tongji University. The table can be input with three-dimensional and six-degree-of-freedom motions. The dimensions of the table are 4 m × 4 m. The working frequency ranges from 0.1 to 50 Hz. The shaking table vibrates with two maximum horizontal direction accelerations of 1.2 g and 0.8 g, and a maximum acceleration of 0.7 g vertically.

2.2. Model soil container

To minimize the box effect, a flexible container was used in the test. The cylindrical soil container was 3000 mm in diameter, see Fig. 1. Its lateral rubber membrane was 5 mm thick, and reinforcement bars having a diameter of 4 mm and spacing of 60 mm were used to strengthen the outside of the box. The membrane was fixed with an upper ring plate and a base plate by bolts. A height-adjustable screw rod was installed to adjust the cylinder to a proper state. A universal joint was set on the top of the columns,

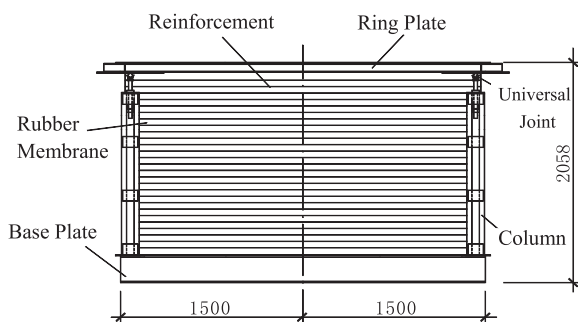


Fig. 1. Schematic diagram of the soil container.

which supported the upper ring plate, to allow the ring plate to deform laterally. To minimize the relative slip between the soil and the container on the base surface, crushed rock was bonded to the base steel plate to roughen the surface. In Ref. [24], Lu et al. conducted three free field-shaking table tests to verify the boundary effect of the flexible container, which was the same one used herein. They indicated that the boundary effect can be ignored when the distance between the structure and the boundary was more than 600 mm. The distance in this paper's tests was more than 1.2 m. Hence, the effect of boundary on dynamic responses of the structure could be ignored.

2.3. Sensors and data acquisition system

To study the dynamic response of the model structure and the dynamic soil–structure interaction, accelerometers, strain gauges, displacement meters, laser displacement meters and soil pressure gauges were used. The strain gauge was an FLA-3-11 produced by the Japanese company TML. The gauge backing was made of epoxy resin with thickness of 0.03 mm, and the length, width, backing length and backing width of the gauge were 0.3, 1.4, 3 and 2 mm, respectively. The laser displacement meter was a CP08MHT80 produced by the German company Wenglor and had dimensions of 50 mm × 50 mm × 20 mm, a measuring range of 50 mm, resolution finer than 8 μm, and response time less than 660 μs. The soil pressure gauge had an outside diameter of 30 mm, capacity of 200 kPa, and precision of 0.5% of full scale. The data acquisition system with 128 channels was produced by MTS Company, and the sampling rate used in the test was 512 Hz.

3. Test design

3.1. Scale factor design

The prototype design of the model structure is a modern subway station with height of 28.3 m. The station was designed originally to be a six-story island platform station, and then because of the need for parking, the first to third floors underground were merged into one layer to function as a stereo garage. The second floor is the lobby floor, the third is a floor that houses equipment, and the fourth is an island platform. The total length of the station is 155 m, and the width varies from 23.6 to 28.35 m. The prototype structure was made of reinforcement concrete. Concrete of Grade C45 was used for central columns and C35 for the rest parts of the station [25]. Steel rebar of HRB400 was used in central columns and HRB335 for the other parts [25].

The scale factors of the model structure are listed in Table 1. According to similarity theory, three aspects of the simulation of the soil–structure interaction should be considered primarily: geometric similarity, physical similarity and mechanical similarity. On account of the differences in dimensions between a modern subway station and typical one, the scale factor design should be based on the size and bearing capacity of the shaking table, size of the soil container, boundary effect, and convenience of model manufacturing. The length scale factor is set to 0.02. Fig. 2 presents the dimensions of the model structure. Then scale factors of displacement and area can be determined.

In the shaking table test, organic glass was chosen as the material of the model structure owing to its good homogeneity, high strength and low elastic modulus, providing flexibility to the design of the scale factor. This material is also suited to accurate manufacturing. Thus elastic modulus and density scale factors can be determined according to material tests of the organic glass.

After the scale factor of geometry, elastic modulus and density are decided, scale factors among the physical quantities can be

Table 1
Scale factors of the model structure.

Type	Physical quantity	Scale factor
Geometry properties	Length	0.020
	Linear displacement	0.020
	Angular displacement	1.000
	Area	4.00×10^{-4}
Material properties	Elastic modulus	0.106
	Equivalent density	1.765
	Stress	0.106
	Strain	1.000
	Poisson's ratio	1.000
Loading	Force	4.24×10^{-5}
	Linear load	2.12×10^{-3}
	Area load	0.106
	Moment	8.48×10^{-7}
	Mass	1.41×10^{-5}
Dynamic properties	Stiffness	2.12×10^{-3}
	Duration	8.16×10^{-2}
	Frequency	12.253
	Velocity	0.245
	Acceleration	3.003

deduced using the Buckingham π law [26]:

$$\begin{cases} S_{\sigma} = S_E \\ S_t = S_l S_{\rho}^{1/2} / S_E^{1/2} \\ S_v = S_E^{1/2} / S_{\rho}^{1/2} \\ S_a = S_E / S_l S_{\rho} \end{cases} \quad (1)$$

where $S_{\sigma}, S_E, S_t, S_l, S_v, S_a$ denote the stress scale factor, elastic modulus scale factor, time scale factor, geometric scale factor, velocity scale factor, and acceleration scale factor, respectively.

According to a numerical simulation of the shaking table test on a subway station [27], the error introduced when using the plane strain hypothesis can be ignored when the distance between the observation plane and the end of the model is equal to the structure width. The widths of the model structure and the column separation are 0.47 and 0.16 m, respectively, and the longitudinal length of the model structure is thus determined to be 1.1 m. A diaphragm wall mainly behaves as a flexural member, as does the central column according to the results of a previous study [28]. In addition, the model structure was designed on the basis of the similarity principle of bending stiffness to introduce the action of steel bars [28]:

$$S_k = S_{\sigma} S_l = \frac{E_p I_p / l_p^3}{E_m I_m / l_m^3} \quad (2)$$

where S_k, S_{σ}, S_l are the stiffness scale factor, stress modulus scale factor, and geometric scale factor, respectively, E_p, I_p, l_p are the prototype's elastic modulus, moment of inertia, and geometry, respectively, and E_m, I_m, l_m are the model's elastic modulus, moment of inertia, and geometry, respectively.

The synthetic model soil was a mixture of sand and sawdust. According to trial tests, adding sawdust to sand can reduce both the density and dynamic shear modulus, which complies with similitude requirements. Employing the Buckingham π law, the scale factors of geometry, density, shear modulus, and inertial acceleration were selected as essential parameters and adjusted to satisfy [26].

$$S_G / (S_l \bullet S_{\rho}) = S_a, \quad (3)$$

where S_G, S_l, S_{ρ}, S_a denote the shear modulus ratio, geometry ratio, density ratio, and inertial acceleration ratio, respectively. The scale factors of soil are presented in Table 2.

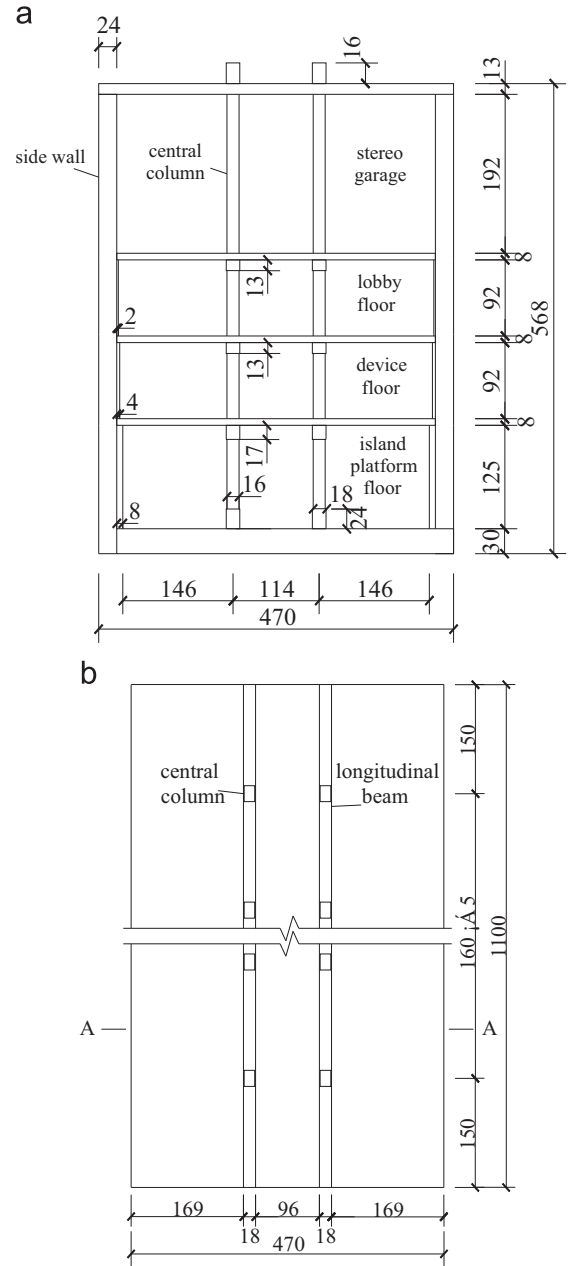


Fig. 2. Dimensions of the model structure: (a) cross section A–A; (b) top view (unit: mm).

Table 2
Scale factors of the model soil.

Physical quantity	Symbols	Scale factor
Shear modulus	S_G	0.020
Length	S_l	0.020
Density	S_{ρ}	0.333
Acceleration	S_a	3.003

3.2. Material and designation of the model

3.2.1. Model structure

To measure the elastic modulus of the organic glass, a material test was carried out as shown in Fig. 3. The elastic moduli of three specimens were 3.60, 3.21, and 3.19 GPa, respectively. The average value was 3.33 MPa, and the corresponding scale factor of the elastic modulus was 0.106. To match the performances of the

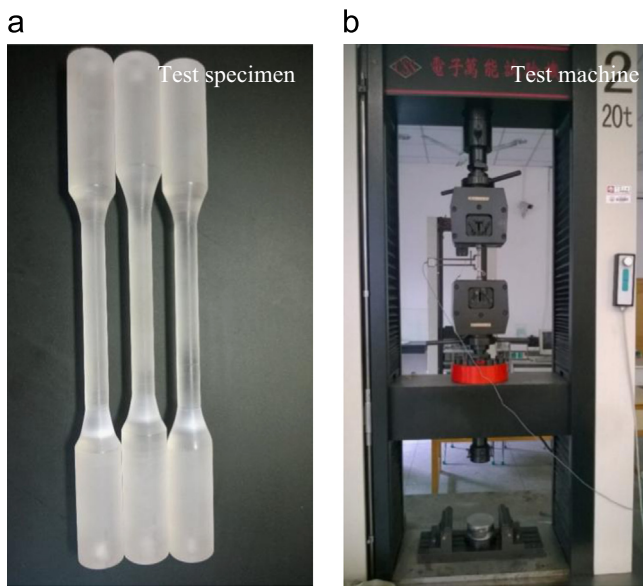


Fig. 3. Material test of organic glass.

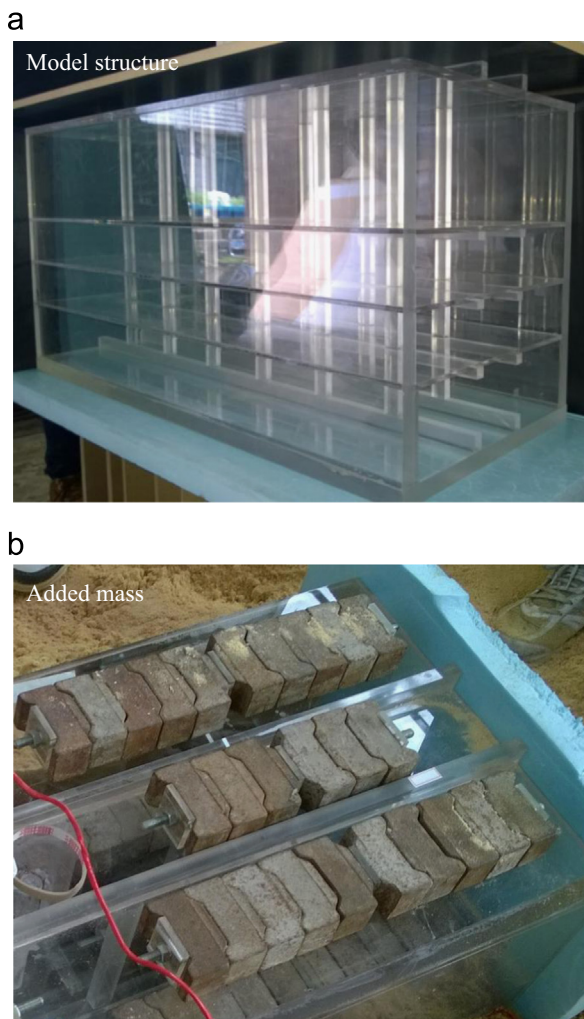


Fig. 4. (a) Model structure; and (b) layout of added mass.

shaking table and to keep the acceleration scale factor and frequency scale factor within reasonable ranges, mass was added to meet the requirement of the density scale factor. When the

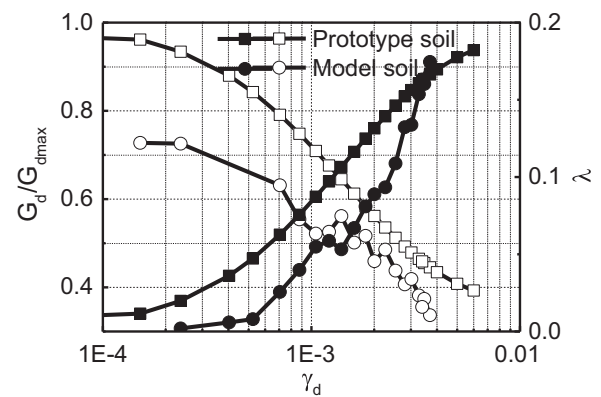


Fig. 5. Dynamic properties of the model soil.

acceleration scale factor is 3.00 and the frequency ratio is 12.253, the density scale factor should be 1.765. In this case, the original model structure mass was 88 kg but should be 324 kg according to the scale factor, and 236 kg of mass thus needed to be added. Owing to the arrangement of sensors, the actual mass added was 208 kg. Fig. 4 shows the layout of added mass.

3.2.2. Model soil

The prototype soil was typical soil deposits found in Shanghai. To satisfy the scale factor equation and taking the maximum dynamic shear modulus, $G_d/G_{d_{max}}-\gamma_d$ curve, and $\lambda-\gamma_d$ curve into consideration, the most appropriate mass ratio of sawdust to sand was 1:2.5, where $G_d, G_{d_{max}}, \lambda, \gamma_d$ denote the dynamic shear modulus, maximum dynamic shear modulus, damping ratio, and dynamic shear strain respectively. The density of the mixture was 700 kg/m^3 , the density scale factor was 0.39, the confining pressure ratio was 0.02, and the modulus obtained in the test was 1.81 MPa (target modulus: 1.72 MPa, error: 5.2%). The $G_d/G_{d_{max}}-\gamma_d$ curve and $\lambda-\gamma_d$ curve obtained in a dynamic tri-axial test are presented in Fig. 5.

During the experiment, the soil was placed into the soil container layer by layer. Each layer was compacted to have thickness of approximately 20 cm. Before the main shaking table test, a trial shaking table test was conducted to analyze the degree of compaction and settlement, and to ensure the soil density in the main test remained accurate and consistent.

3.3. Layouts of sensors

Fig. 6 presents the soil container and observation plane. The layouts of 20 strain gauges, 18 accelerometers, 10 displacement meters, eight laser displacement meters, and 10 soil pressure gauges in the model soil and model structure are shown in Figs. 7 and 8. Strain gauges were used to investigate the dynamic response of the structure. Accelerometers A3, A6, A9, and A12 were set to investigate the propagation law of seismic waves in soil, accelerometers A2, A5, A8, and A11 to investigate the effect of structure on the propagation law, accelerometers A10, A11, and A12 to validate the boundary effect, and accelerometers A15–A18 to record the dynamic acceleration response of each story. Displacement meters were placed to measure the settlement of soil and lateral displacement of the soil container. Laser displacement meters were fixed on the upper surface of each floor and circular tubes made of organic glass were fixed on the lower surface of each floor. Hence, the laser displacement meters provided data on the relative displacement of the central column and side wall. Soil pressure gauges P1–P8 were arranged to explore the distribution of the dynamic earth pressure and P9 and P10 were used to check the dynamic earth pressure.

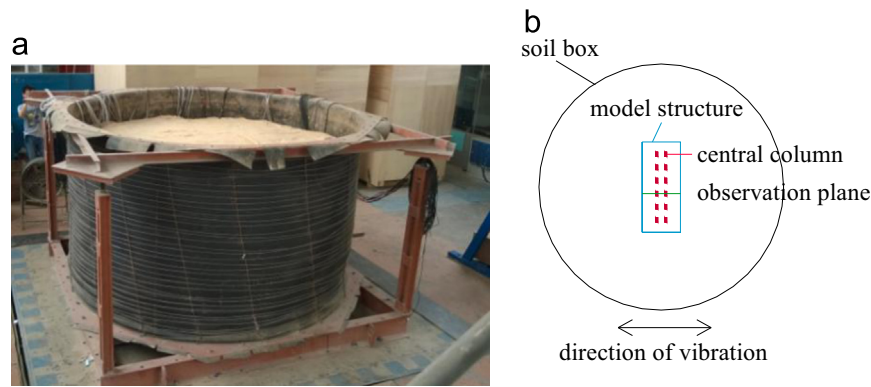


Fig. 6. (a) Soil container; and (b) location of the observation plane.

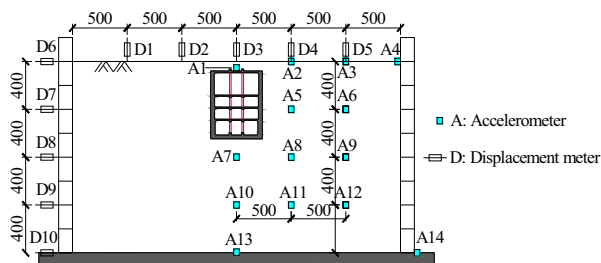


Fig. 7. Layouts of accelerometers embedded in soil and displacement meters (unit: mm).

3.4. Loading method and test cases

To investigate the effect of pulse-like ground motion on the subway station, three records were selected from the Pacific Earthquake Engineering Research Center database [29] and the information is shown in Table 3. Specifically, El Centro ground motion is ordinary ground motion while Hector Mine and ChiChi ground motions are pulse-like ground motions. Definitions of pulse-like ground motion are consistent with those given by the papers [30,31]. To define the pulse-like characteristics of these motions more directly, the ratio of peak ground velocity to peak ground acceleration (PGV/PGA) was selected as the index. According to studies [11,32], pulse-like ground motion is defined as ground motion whose PGV/PGA is greater than 0.2 while ordinary ground motion has a ratio smaller than 0.15. The pulse-like effect of Hector Mine ground motion is greater than that of ChiChi ground motion. Fig. 9 presents the acceleration time histories and Fourier spectra of the three records.

For the purpose of investigating the dynamic earth pressure under different intensities and types of ground motions, the three ground motions were scaled to four levels (0.1, 0.2, 0.6, and 1.0 g). White noise was used to check the changes in the model. Table 4 gives the test cases.

4. Test verification

4.1. Amplification of the acceleration of soil

According to tests results, peak values of accelerometers A7, A8 and A9 under El Centro ground motion (peak acceleration was 0.1 g) were 0.085, 0.081 and 0.082, respectively (see Fig. 10), which indicated that influences of boundary effect could be ignored.

Fig. 11 presents the peak acceleration amplification factors for different depths of soil with different peak accelerations. Because there was no signal for A12, it is replaced by the signal for A11 temporarily in Fig. 11. It is seen that, when peak acceleration were

Table 3
Input ground motions.

Information	Ground motion		
	Hector Mine	ChiChi	El Centro
PGA (g)	0.1	0.1	0.1
PGV (m/s)	0.766	0.496	0.115
PGV/PGA (s)	0.766	0.496	0.115
Record sequence number	1803	1542	172

0.1 g and 0.2 g, the amplification factors were greater closer to the ground surface. Additionally, amplification factors at any depth under pulse-like ground motion were slightly larger than those under ordinary ground motion. However, in the case of 0.6 g, the amplification factors were obviously lower. Huang et al. [33], in their study of the dynamic response of soil deposits in Shanghai, found that soil had damping characteristics when the peak acceleration of the input wave was larger than 0.3 g. In this paper, methods proposed by Zeghal et al. [34] and Brennan et al. [35] were used to calculate the shear modulus and damping ratios of the soil. It is found that with the increase of acceleration, shear modulus decreases significantly, resulting in the natural frequency getting far away from the domain frequency of the motion. This might cause a reduction in amplification factor of soil acceleration.

The peak acceleration of the model structure is shown in Fig. 12. Generally, the model structure embedded in soil underwent the magnified acceleration effect. The accelerations of different stories were magnified to various degrees. The peak accelerations recorded by A16 and A17 were much higher than those recorded by other accelerometers. The effect of different types of ground motion on the peak accelerations of the structure is not clear.

4.2. Lateral displacement and settlement of soil

Fig. 13 shows the maximum lateral displacements of the soil container under different ground motions with the peak acceleration of 0.1 g. To better understand the lateral displacement of the soil container under ground motions, typical time histories of displacement meter D6 are presented in Fig. 13(b). Fig. 13(a) shows shear-type deformation of the soil container, which satisfies the lateral deformations of soils as semi-infinite half space media subjected to the ground motion of a real earthquake [36]. In addition, it could be find from Fig. 13(a) and (b) that the effect of the pulse-like ground motion on the overall soil deformation was much greater than that of ordinary ground motion.

Taking the record of the Hector Mine ground motion as an example, Fig. 14(a) shows the instantaneous soil deformation under the Hector Mine ground motion when the peak acceleration was 0.1 g. In Fig. 14, T symbol stands for the duration of earthquakes. It is

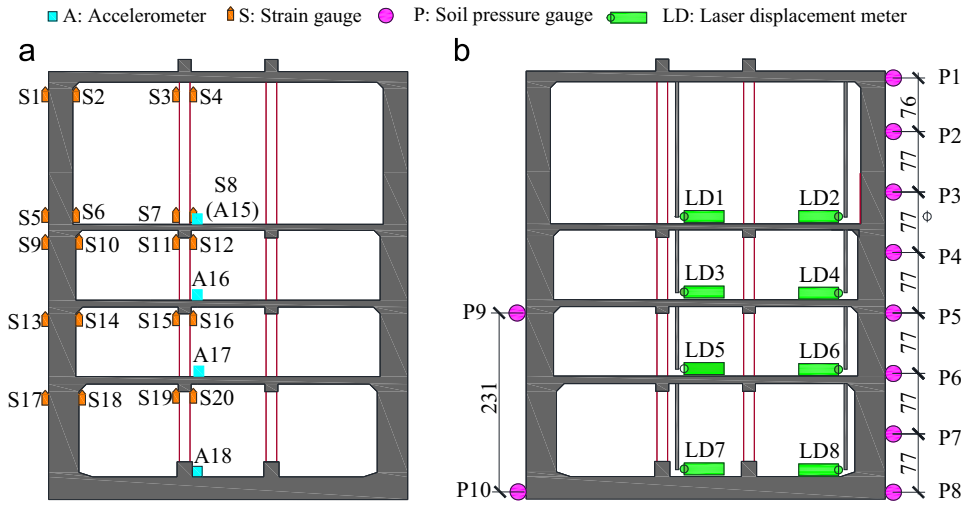


Fig. 8. Layouts of sensors on the cross section of the model structure: (a) accelerometers and strain gauges; and (b) soil pressure meters and laser displacement meters.

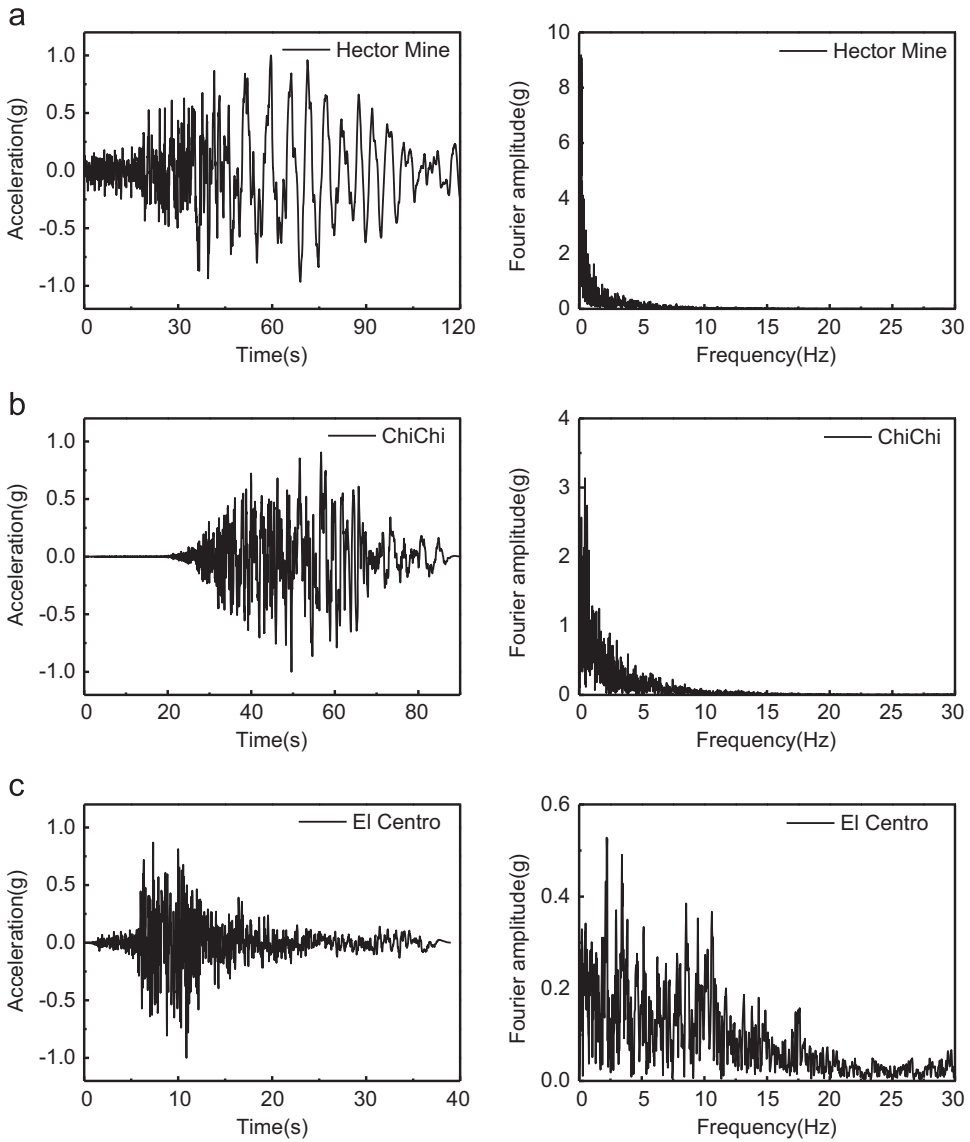


Fig. 9. Acceleration-time histories and Fourier spectra of (a) Hector mine, (b) ChiChi, and (c) El Centro ground motions.

seen that the container had a shear-type deformation mode throughout the duration of the earthquake. Fig. 14(b) shows the maximum soil deformation under the Hector Mine ground motion with different peak accelerations. It can be concluded that the deformations were large close to the ground, especially when the earthquake was strong. Moreover, owing to the large story height of the first floor underground, this kind of deformation can do more harm to the subway station. In the actual project, the density of soil near the surface is lower than that at greater depth, and the deformation of soil near the surface might thus be even larger.

Table 4
Test program.

Test sequence	Test no.	Ground motion	Peak acceleration (g)
1	WN-1	White Noise	0.07
2	El-x0.1	El Centro	0.10
3	Chi-x0.1	ChiChi	0.10
4	HM-x0.1	Hector Mine	0.10
5	WN-2	White Noise	0.07
6	El-x0.2	El Centro	0.20
7	Chi-x0.2	ChiChi	0.20
8	HM-x0.2	Hector Mine	0.20
9	WN-3	White Noise	0.07
10	El-x0.6 g	El Centro	0.60
11	Chi-x0.6 g	Hector Mine	0.60
12	HM-x0.6	ChiChi	0.60
13	WN-4	White Noise	0.07
14	El-x1.0 g	El Centro	1.00
15	Chi-x1.0 g	ChiChi	1.00
16	HM-x1.0	Hector Mine	1.00

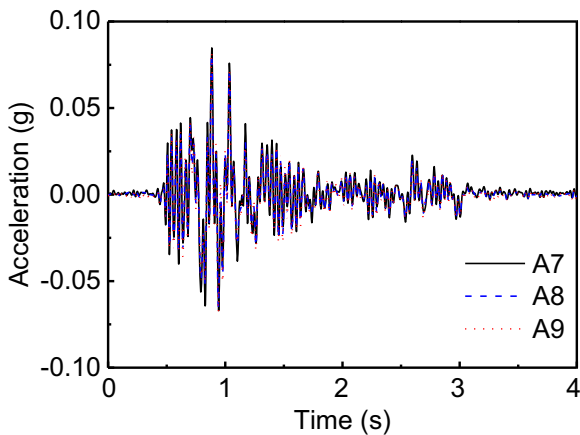


Fig. 10. Time histories of accelerometers A7, A8 and A9 under El Centro ground motion with peak acceleration of 0.1 g.

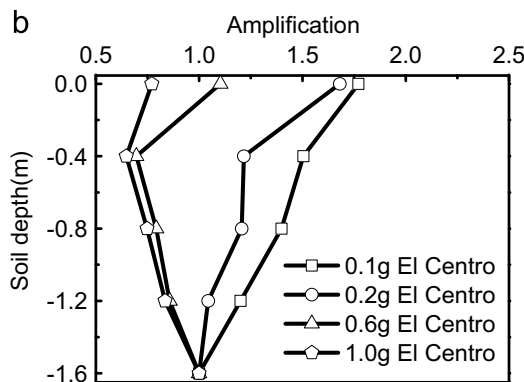
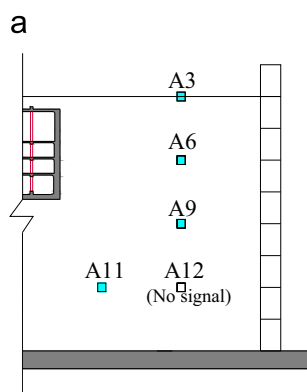


Fig. 11. Peak acceleration amplification factors of the model soil.

In the test, the obvious settlement of soil implies a significant change in the soil density, which may affect the test results. Fig. 15 shows the maximum settlements of soil for the three records with

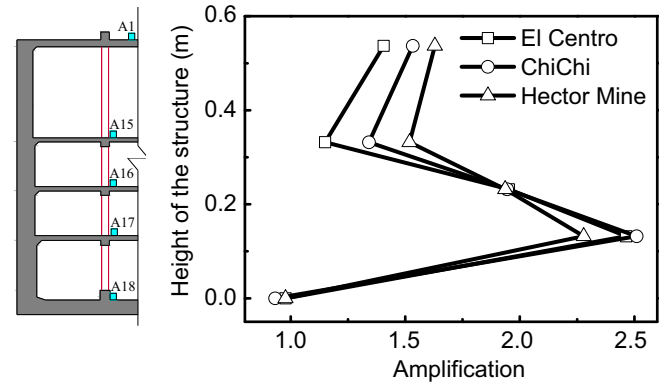


Fig. 12. Peak acceleration amplification factors of the model structure.

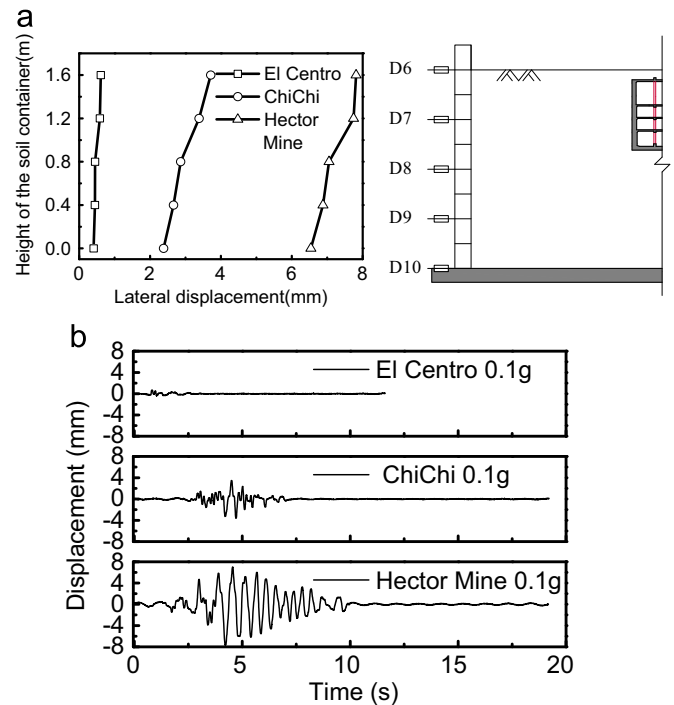


Fig. 13. Lateral displacements of the model soil container under different ground motions and (b) time history of lateral displacement of D6.

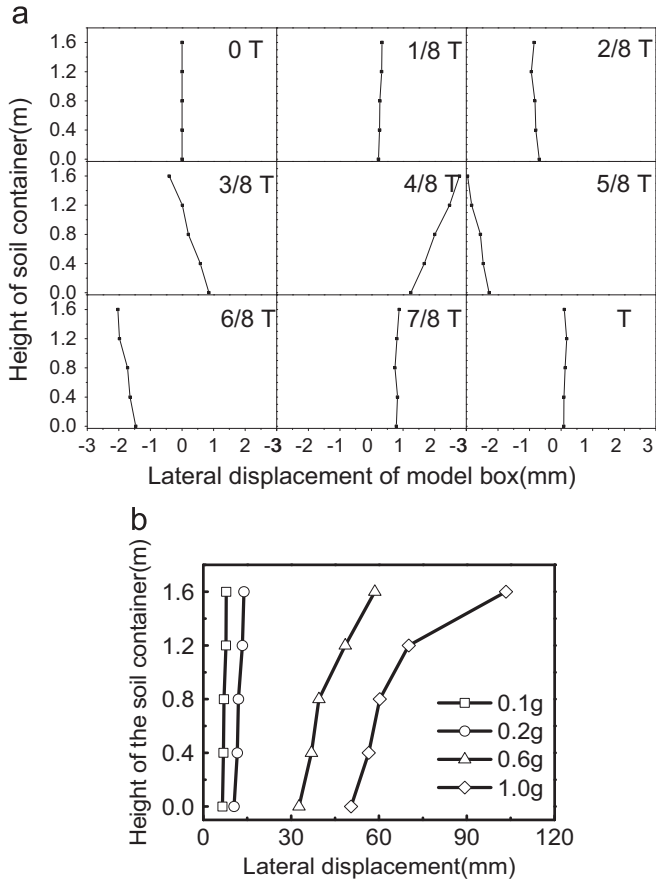


Fig. 14. Lateral displacements of the model soil container under the Hector Mine ground motion (a) in steps of one-eighth of the duration of the ground motion; (b) with different peak accelerations.

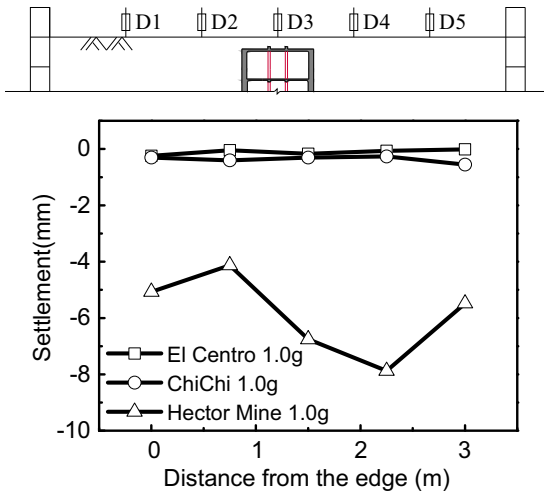


Fig. 15. Settlement of the model soil under three ground motions when peak accelerations are 1.0g.

the maximum peak acceleration. It is concluded that the changes in density can be ignored. Under the El Centro and ChiChi ground motions, the maximum settlement was less than 1.0 mm. In the case of the Hector Mine record, the maximum settlement was 7.8 mm, which is small compared with the height of the soil, 1.6 m. In particular, the effect of strong pulse-like ground motion (in the Hector Mine record) on the settlement of soil was much stronger than the effects of ground motion in the El Centro and ChiChi records. This difference in settlement was caused by the energy of

ground motions. Hector Mine ground motion carries much larger energy than El Centro, which will be explained in detail later.

5. Test result and analysis

5.1. Deformation mode of the model structure

The presented results of displacements, accelerations, and soil pressures mean dynamic results. Internal forces presented include both static and dynamic forces. To comply with the real project, all results obtained in the test were converted from model to prototype according to the scale factors. As shown in Fig. 16, the model structure had a racking deformation mode. In Fig. 16, *T* symbol stands for the duration of earthquakes. Fig. 16(a) presents the instantaneous deformation of the side wall in steps of one-fourth of the period of the El Centro record when the peak acceleration was 0.033 g. Fig. 16(b) shows the maximum deformation of the side wall throughout the entire period under different records with different peak accelerations.

Both the instantaneous and maximum deformations of the side wall turned out to have a nice racking form, especially when the peak acceleration was small. When subjected to shear distortions during an earthquake, a rectangular box structure will undergo transverse racking deformation [37]. Although the multi-story subway station has relatively large height, it still has a nice racking deformation mode. This is mainly because of the large stiffness imparted by its thick side wall. Chen et al. [38] came to the same conclusion on the basis of numerical results. The deformations increased with the peak acceleration. By comparing the deformations under the El Centro ground motion with those under the ChiChi and Hector Mine ground motions, it is found that the deformations of the side wall under pulse-like ground motions were obviously larger than those under ordinary ground motions. Comparison between the deformations for the ChiChi record with those for the Hector Mine record shows that the pulse-like effect may remarkably increase the seismic response of the understructure.

5.2. Dynamic response characteristics of the internal force of the central column

Fig. 17 shows the relationship between the maximum moment of the top-story central column and the peak acceleration of input motions.

The maximum moment of the central column on the top story increased with the peak acceleration. The maximum moments under pulse-like ground motions were obviously larger than those under ordinary ground motions. The maximum moment increased with the magnitude of the pulse-like effect. In addition, the pulse-like effect is remarkable especially in a destructive earthquake. In Fig. 17, when the peak acceleration was 0.033 g, the maximum moment of the first-story central column induced by the Hector Mine (ChiChi) ground motion was 26.44% (20.20%) larger than that induced by the El Centro ground motion. When the peak acceleration was 0.333 g, the difference reached 80.64% (29.43%).

The above results are mainly explained as follows. First, although seismic waves have the same peak acceleration, pulse-like ground motion carries more energy than the ordinary motion. Various parameters are used to measure earthquake energy. The Arias intensity [39] is an important measure of the strength of ground motion, as it simultaneously reflects multiple characteristics of the motion [40]. The Arias intensity describes the cumulative energy per unit weight absorbed by an infinite set of single-degree-of-freedom oscillators [41]. Moustafa and Takewaki [42] used the Arias intensity to describe the characteristics of pulse-like motions.

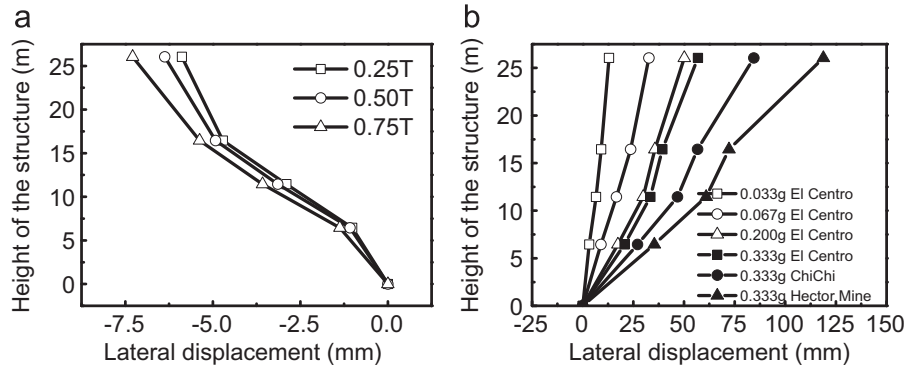


Fig. 16. Lateral displacements of the side wall (a) in steps of one-fourth of the ground motion duration; and (b) under three ground motions.

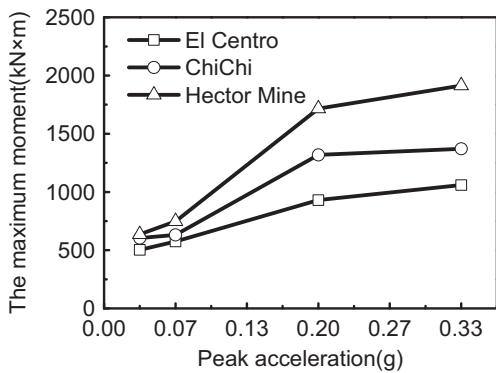


Fig. 17. Maximum moment of the top-story central column.

Calculations show that when the peak acceleration is 0.1 g, the Arias intensity of the El Centro, ChiChi, and Hector Mine ground motions are 0.146, 0.773, and 2.113, respectively. There is clearly a great difference in energy among the three motions. Second, the pulse-like ground motions are rich in low-frequency components if compared with the ordinary ground motion, as seen for the Fourier spectrum of the three ground motions in Fig. 9. The soil deposits filter out a significant portion of the high-frequency content and can amplify low-frequency signals. As a result, when seismic waves propagate from bedrock to the underground structure, the energy attenuation of pulse-like motion is less than that of ordinary motion. Therefore, the input energy of the underground structure is dramatically different. A large proportion of the energy of ordinary motion is dissipated by soil.

To evaluate the safety of the subway station under different intensities and types of ground motions, the top-story central column was selected as an observed object for two reasons. First, the large story height of the top story means that the lateral stiffness is much lower for the top story than for the other stories. Second, although the axial force of the bottom-story column is the largest, the size of the top-story column is relatively small and thus the bearing capacity is relatively low. Axial force–moment time histories with peak acceleration of 0.333 g converted from model to prototype and axial force–moment bearing capacity curves calculated for the prototype are presented in Fig. 18. With the same peak acceleration, the Hector Mine motion, followed by ChiChi motion and then El Centro motion, had the greatest effect on the moment. The prototype structure is made of reinforced concrete (an elasto-plastic material), while the model structure is made of organic glass (an elastic material). However, from the point of dynamic internal forces, the stress concentration of the prototype structure may affect distributions of internal forces thus leading to higher forces in some sections compared to the elastic responses. Moreover, nonlinearities of soils and interface which

affected by the flexibility of the structure will also change the elastic internal forces of central columns [43]. In addition, Piti-lakis and Tsinidis [44] pointed out that the displacement-based methods were closer to the physics of the problem and presented several advantages including the proper evaluation of the inelastic response of the structural components. Consequently, using deformations to describe the columns performance will be more rational, and will also show the kinematic nature.

In addition, with respect to the effects of motions on the axial force, there are few differences between pulse-like motions and ordinary motions. As shown in Fig. 18, the maximum axial forces of the top-story central column under El Centro, ChiChi, and Hector Mine ground motions were 4330, 4160, and 4390 kN, respectively. Moreover, the conclusion is transferable to bottom-story columns. It is found that under two extreme conditions (0.033-g El Centro ground motion and 0.333-g Hector Mine ground motion), there was only a 401-kN (1.2%) difference in the axial compression ratio. In other words, the horizontal inputted pulse-like motion did not induce vertical vibration of the central column.

5.3. Dynamic response characteristics of the displacement of the central column

Column drifts of each story under the ChiChi ground motion with different peak accelerations are shown in Fig. 19. It can be concluded from the gradient in the figure that (1) the drift increased with the peak acceleration and (2) except in the 0.066-g case, the column drifts of the top story and the bottom story were larger than those of the middle stories. For instance, when the peak acceleration was 0.333 g, the column drift for the top story was 37.68% higher than that for the second story. The lateral stiffness values of columns on the top story and second story were 4.71×10^6 and 6.07×10^7 N/m, respectively. An increase in height clearly reduced the lateral stiffness, therefore enlarging the column drift.

As stated in the previous section, from the perspective of internal forces, central columns seemed safe under the ground motions of the considered earthquakes. But it did not take account of stress concentration effect and so on. From the view of performance-based design, deformation is a more suitable index than force with which to evaluate the seismic performance of underground structures. In investigating the relationship between the pulse-like effect and column drift, the top-story central column was selected for its large story height. Fig. 20 shows the relation between the column drift and peak acceleration. The variation in column drift was basically the same as that of the moment: (1) the column drift on the top story increased with the peak acceleration; (2) the column drift under pulse-like ground motion was obviously larger than that under ordinary ground motion and increased with an increase in the

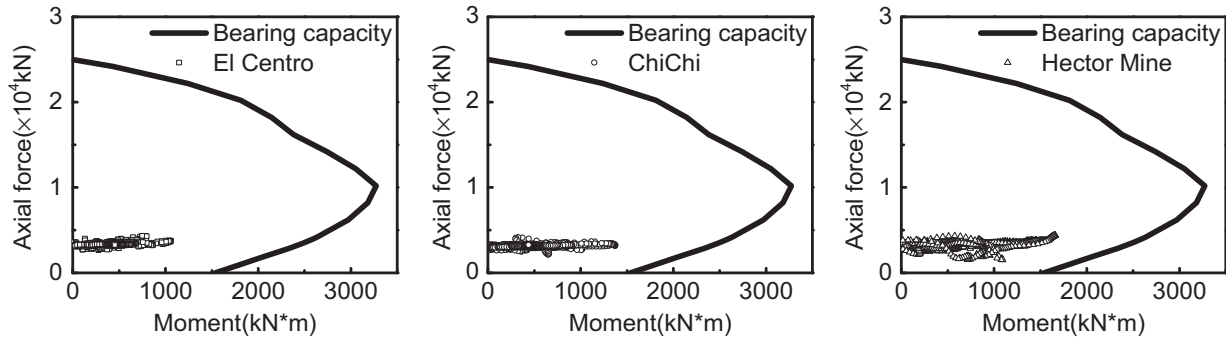


Fig. 18. Bearing capacity curves and axial force–moment time histories of the top-story central column with peak acceleration of 0.333 g.

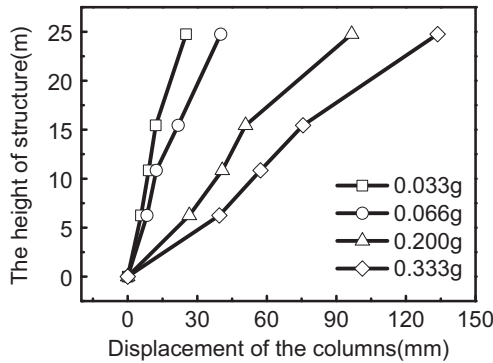


Fig. 19. Lateral displacements of columns in each story under ChiChi ground motion.

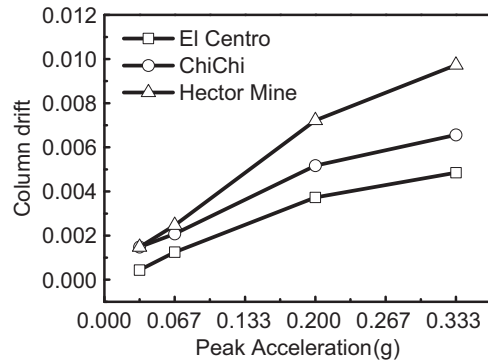


Fig. 20. Column drifts of the top-story central column.

magnitude of the pulse-like effect; and (3) such increment was greater given the peak acceleration was higher; i.e., the earthquake imposed was stronger.

As stated in the previous section, from the perspective of internal forces, central columns were safe under the ground motions of the considered earthquakes. This does not entirely agree with the perspective of deformation. Table 5 presents the top-story column drift under the three motions with different peak accelerations. When the peak acceleration of prototype was 0.2 g (major earthquake), column drifts were already beyond 1/200. Furthermore, when the peak acceleration was 0.333 g, the column drift reached 1/103 under Hector Mine ground motion. It is important to note that, because the model structure is elastic, the column drifts measured are smaller than those in a real situation. Hence, the column drift rather than the internal force deserves more attention and improvement.

5.4. Dynamic earth pressure distribution

Fig. 21 shows the maximum dynamic earth pressure distribution on the model structure. The dynamic earth pressure was calculated by subtracting the static earth pressure from the total earth pressure. It is seen that the dynamic earth pressure under pulse-like motion was higher than that under ordinary motion. However, the maximum dynamic earth pressure distribution was not clear and it is different from the dynamic earth pressure acting on a single-double story or double-story underground structure [27,45,46]. Additionally, the distribution mode with an “S” shape is inconsistent with the pressure induced by racking deformation. Nonlinear phenomena of soils and the soil–structure interface during shaking, especially for higher intensities, may also affect the dynamic earth pressure. Additionally, these recorded earth pressures may be biased to some extent by the response of the earth pressure cells. Tsinidis et al. [47] also stated that the relative

Table 5
Column drifts of the top-story central column.

Peak acceleration of model structure	Peak acceleration of prototype structure	Column drift of the top-story central column		
		El Centro	ChiChi	Hector Mine
0.1 g	0.033 g	1/2278	1/677	1/677
0.2 g	0.066 g	1/797	1/482	1/404
0.6 g	0.200 g	1/268	1/193	1/138
1.0 g	0.333 g	1/206	1/153	1/103

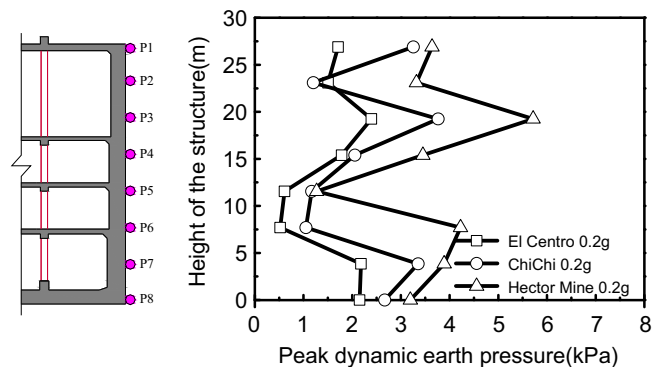


Fig. 21. Distribution of the peak dynamic soil pressure on the side wall.

stiffness of the sensing plate may affect the readings of earth pressure cells. And the responses of pressure gauges can be quite tricky in cases of dry cohesionless soils due to grain size effects and so on.

6. Conclusions

Shaking table tests were conducted to study the effect of pulse-like ground motions on a multi-story modern subway station. The following conclusions are drawn from the results of the study.

- (1) Because of the strength of low-frequency components and high energy, pulse-like ground motion has a dramatically greater dynamic effect than ordinary motion on underground structures and surrounding soils, in terms of the internal forces and drift of the central column and deformation of the side wall and soil.
- (2) The multi-story subway station operates in a racking deformation mode.
- (3) Central columns, especially columns with large height, are the points vulnerable to ground motion. Reducing the lateral stiffness generated by large story height increases the column drift notably. The column may suffer larger dynamic responses under pulse-like ground motion than under ordinary ground motion. When the peak acceleration of input motion is 1.0 g, the top-story maximum moment and drift under strong pulse-like ground motion are 81% and 100% higher than those under ordinary ground motion, respectively.

Acknowledgments

This research was supported by the State Key Laboratory of Disaster Reduction in Civil Engineering (SLDRCE14-B-11), National Natural Science Foundation of China (Grant no. 51278524 and Grant no. 41472246), and Innovation Program of Shanghai Municipal Education Commission (14ZZ034). The experimental program carried out in this research could not have been executed without the able assistance of Lu Wensheng and Zhao Bin of the State Key Laboratory. All support is gratefully acknowledged.

References

- [1] Wang W, Zhao GG. 71 m! "The Iron Giant" sets new record on "the Shanghai depth". Wen Hui Bao Newspaper; 2013. 09:1. [In Chinese].
- [2] Tamari Y, Towhata I. Seismic soil–structure interaction of cross sections of flexible underground structures subjected to soil liquefaction. *Soils Found* 2003;43(2):69–87.
- [3] Kutter BL, Chou JC, Travarasou T. Centrifuge testing of the seismic performance of a submerged cut-and-cover tunnel in liquefiable soil. In: Proceedings of the geotechnical earthquake engineering and soil dynamics IV congress (GSP); 2008. 181.
- [4] Chen GX, Wang ZH, Zuo X, Du XL, Gao HM. Shaking table test on the seismic failure characteristics of a subway station structure on liquefiable ground. *Earthq Eng Struct Dyn* 2013;42(10):1489–507. <http://dx.doi.org/10.1002/eqe.2283>.
- [5] Moss RES, Crosariol VA. Scale model shake table testing of an underground tunnel cross section in soft clay. *Earthq Spectra* 2013;29(4):1413–40. <http://dx.doi.org/10.1193/070611EQS162M>.
- [6] Kagawa T, Sato M, Minowa C, Abe A, Tazoh T. Centrifuge simulations of large-scale shaking table tests: case studies. *J Geotech Geoenviron Eng* 2004;130(7):663–72.
- [7] Kamata H, Mashimo H. Centrifuge model test of tunnel face reinforcement by bolting[J]. *Tunn Undergr Space Technol* 2003;18(2):205–12.
- [8] Pitilakis D, Dietz M, Wood DM, Clouteau D, Modaresi A. Numerical simulation of dynamic soil–structure interaction in shaking table testing. *Soil Dyn Earthq Eng* 2008;28(6):453–67.
- [9] Chen GX, Chen S, Zuo X, Du XL, Qi CZ, Wang ZH. Shaking-table tests and numerical simulations on a subway structure in soft soil. *Soil Dyn Earthq Eng* 2015;76:13–28.
- [10] Chen J, Shi X, Li J. Shaking table test of utility tunnel under non-uniform earthquake wave excitation. *Soil Dyn Earthq Eng* 2010;30(11):1400–16.
- [11] Loh CH, Wan S, Liao WL. Effects of hysteretic model on seismic demands: consideration of near-fault ground motions. *Struct Des Tall Build* 2002;11(3):155–69. <http://dx.doi.org/10.1002/tal.182>.
- [12] Somerville P, Graves R. Conditions that give rise to unusually large long period ground motions. *Struct Des Tall Build* 1993;2(3):211–32.
- [13] Wen WP, Zhai CH, Li S, Chang ZW, Xie LL. Constant damage inelastic displacement ratios for the near-fault pulse-like ground motions. *Eng Struct* 2014;59:599–607. <http://dx.doi.org/10.1016/j.engstruct.2013.11.011>.
- [14] Bertero VV, Mahin SA, Herrera RA. Aseismic design implications of near-fault San Fernando earthquake records. *Earthq Eng Struct Dyn* 1978;6(1):31–42.
- [15] Anderson JC, Bertero VV. Uncertainties in establishing design earthquakes. *J Struct Eng* 1987;113(8):1709–24.
- [16] Makris N, Black CJ. Evaluation of peak ground velocity as a "good" intensity measure for near-source ground motions. *J Eng Mech* 2004;130(9):1032–44. [http://dx.doi.org/10.1061/\(ASCE\)0733-9399\(2004\)130:9\(1032\)](http://dx.doi.org/10.1061/(ASCE)0733-9399(2004)130:9(1032)).
- [17] Sehhati R, Rodriguez-Marek A, ElGawady M, Cofer WF. Effects of near-fault ground motions and equivalent pulses on multi-story structures. *Eng Struct* 2011;33(3):767–79. <http://dx.doi.org/10.1016/j.engstruct.2010.11.032>.
- [18] Makris N, Chang SP. Effect of viscous, viscoplastic and friction damping on the response of seismic isolated structures. *Earthq Eng Struct Dyn* 2000;29(1):85–107.
- [19] Jangid R, Kelly JM. Base isolation for near-fault motions. *Earthq Eng Struct Dyn* 2001;30(5):691–707. <http://dx.doi.org/10.1002/eqe.31>.
- [20] Hall JF, Heaton TH, Halling MW, Wald DJ. Near-source ground motion and its effects on flexible buildings. *Earthq Spectra* 1995;11(4):569–605.
- [21] Ismail M, Casas JR. Novel isolation device for protection of cable-stayed bridges against near-fault earthquakes. *J Bridge Eng* 2014;19(8). [http://dx.doi.org/10.1061/\(ASCE\)BE.1943-5592.0000509](http://dx.doi.org/10.1061/(ASCE)BE.1943-5592.0000509).
- [22] Phan V, Saeidi MS, Anderson J, Ghasemi H. Near-fault ground motion effects on reinforced concrete bridge columns. *J Struct Eng* 2007;133(7):982–9. [http://dx.doi.org/10.1061/\(ASCE\)0733-9445\(2007\)133:7\(982\)](http://dx.doi.org/10.1061/(ASCE)0733-9445(2007)133:7(982)).
- [23] Chen ZY, Wei JS. Correlation between ground motion parameters and lining damage indices for mountain tunnels. *Nat Hazards* 2013;65(3):1683–702. <http://dx.doi.org/10.1007/s11069-012-0437-5>.
- [24] Lu XL, Li PZ, Chen YQ, Chen B. Chen Shaking table model testing on dynamic soil–structure interaction system. In: Proceedings of the 13th world conference on earthquake engineering; 2004. p. 1–16.
- [25] GB50010. Code for design of concrete structure. Beijing: China Architecture & Building Press; 2010.
- [26] Moncarz PD, Krauwinkler H. Theory and application of experimental model analysis in earthquake engineering. Report No. 50. Stanford, CA: Dept. of Civil Engineering and Environmental Engineering, Stanford University; 1981.
- [27] Yang LD, Yang C, Ji QQ, Zheng YL. Shaking table test and numerical calculation on subway station structures in soft soil. *J Tongji Univ* 2003;31(10):1135–40.
- [28] Lin G, Zhu T, Lin B. Similarity technique for dynamic structural model test. *J Dalian Univ Technol* 2000;40(1):1–8.
- [29] Pacific Earthquake Engineering Research Center (PEER). PEER strong motion database. Berkeley: University of California; 2000.
- [30] Baker JW. Quantitative classification of near-fault ground motions using wavelet analysis. *Bull Seism Soc Am* 2007;97(5):1486–501. <http://dx.doi.org/10.1785/0120060255>.
- [31] Shahi SK, Baker JW. An empirically calibrated framework for including the effects of near-fault directivity in probabilistic seismic hazard analysis. *Bull Seism Soc Am* 2011;101(2):742–55. <http://dx.doi.org/10.1785/0120100090>.
- [32] Bray JD, Rodriguez-Marek A. Characterization of forward-directivity ground motions in the near-fault region. *Soil Dyn Earthq Eng* 2004;24(11):815–28. <http://dx.doi.org/10.1016/j.soildyn.2004.05.001>.
- [33] Huang Y, Ye WM, Chen ZC. Seismic response analysis of the deep saturated soil deposits in Shanghai. *Environ Geol* 2009;56(6):1163–9. <http://dx.doi.org/10.1007/s00254-008-1216-1>.
- [34] Zeghal M, Elgamal AW, Tang HT, Stepp JC. Lotung downhole array. II: evaluation of soil nonlinear properties. *J Geotech Eng* 1995;121(4):363–78.
- [35] Brennan AJ, Thusyanthan NI, Madabhushi SPG. Evaluation of shear modulus and damping in dynamic centrifuge tests. *J Geotech Geoenviron Eng ASCE*, 131; 2005. p. 1488–97.
- [36] Meymand P. Shaking table scale model test of nonlinear soil–pile–superstructure interaction in soft clay [PhD dissertation]. Berkeley: University of California; 1998.
- [37] Hashash YMA, Hook JJ, Schmidt B, Yao JIC. Seismic design and analysis of underground structures. *Tunn Undergr Space Technol* 2001;16(4):247–93. [http://dx.doi.org/10.1016/S0886-7798\(01\)00051-7](http://dx.doi.org/10.1016/S0886-7798(01)00051-7).
- [38] Chen ZY, Chen W, Zhang W. Zhang Seismic performance evaluation of multi-story subway structure based on pushover analysis. *Advances in Soil Dynamics and Foundation Engineering (ASCE)*; 2014. p. 444–54.
- [39] Arias A. Measure of earthquake intensity. Massachusetts Inst. of Tech., Cambridge. Univ. of Chile, Santiago de Chile; 1970.
- [40] Stafford P, Berrill J, Pettinga J. New predictive equations for Arias intensity from crustal earthquakes in New Zealand. *J Seism* 2009;13(1):31–52. <http://dx.doi.org/10.1007/s10950-008-9114-2>.
- [41] Travarasou T, Bray JD, Abrahamson NA. Empirical attenuation relationship for Arias intensity. *Earthq Eng Struct Dyn* 2003;32(7):1133–55. <http://dx.doi.org/10.1002/eqe.270>.
- [42] Moustafa A, Takewaki I. Deterministic and probabilistic representation of near-field pulse-like ground motion. *Soil Dyn Earthq Eng* 2010;30(5):412–22. <http://dx.doi.org/10.1016/j.soildyn.2009.12.013>.
- [43] Lanzano G, Bilotta E, Russo G, Silvestri F, Madabhushi SPG. Centrifuge modeling of seismic loading on tunnels in sand. *Geotech Test J* 2012;35(6):854–69.
- [44] Pitilakis K, Tsiniadis G. Performance and seismic design of underground structures. *Earthq Geotech Eng Des* 2014;28:279–340 Geotechnical Geological and Earthquake Engineering, Springer.

- [45] Zhai E, Davis CA, Yan LP, Hu JP. Numerical simulations of geotechnical centrifuge modeling of seismic earth pressures on an underground restrained structure. International efforts in lifeline earthquake engineering. In: Proceedings of the 6th China–Japan–US trilateral symposium on lifeline earthquake engineering; 2014. p. 369–76. DOI: 10.1061/9780784413234.048.
- [46] Jiang LZ, Chen J, Li J. Seismic response of underground utility tunnels: shaking table testing and FEM analysis. *Earthq Eng Eng Vib* 2010;9(4):555–67.
- [47] Tsinidis G, Pitilakis K, Madabhushi G, Heron C. Dynamic response of flexible square tunnels: centrifuge testing and validation of existing design methodologies. *Geotechnique* 2015;65:401–17.